SOME STUDIES ON THE NONLINEAR DYNAMIC RESPONSE OF SHELL-TYPE STRUCTURES

By David A. Evensen and Robert E. Fulton

NASA Langley Research Center
Langley Station, Hampton, Va.

Presented to the International Conference on
Dynamic Stability of Structures

Evanston, Illinois
October 18-20, 1965

SOME STUDIES ON THE NONLINEAR DYNAMIC RESPONSE OF SHELL-TYPE STRUCTURES

By David A. Evensen and Robert E. Fulton

NASA Langley Research Center

INTRODUCTION

Recent aerospace applications involving thin-walled structures have necessitated studies of the nonlinear vibration and response of thin shells. The results of some current research on nonlinear dynamics of thin shells are summarized in the present paper. Two related problem areas are outlined; both involve geometric nonlinearities and thin shells of revolution.

The first problem considered is the forced, nonlinear flexural vibrations of thin-walled circular cylinders. Approximate solutions are obtained which show that vibrations involving a single bending mode or two coupled bending modes can occur. The analysis exhibits several features that are characteristic of nonlinear flexural vibrations of axisymmetric elastic structures in general.

The second problem deals with the dynamic axisymmetric snap-through buckling of shallow conical and spherical shells subjected to uniformly distributed impulsive pressures. Approximate buckling pressures are obtained for a variety of boundary conditions for both types of shells and comparisons are made between conical and spherical caps having similar geometries.

SYMBOLS

$A_n(t), B_n(t)$ generalized coordinates

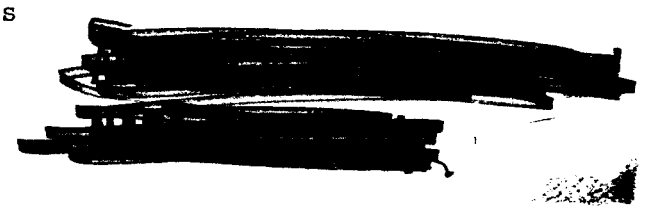

$\overline{A},\overline{B}$	average values (over one period) of the vibration amplitudes (see eqs. (7) and (9))
b	external radius of conical shell (fig. 7a)
D	bending stiffness, $\frac{Eh^3}{12(1-\mu^2)}$
E	Young's modulus
F(x,y,t)	stress function
G_{mn}	nondimensional amplitude of the applied loading
h	shell thickness
H	center rise of the shell (figs. 7a and 7b)
I	initial impulse parameter, $\frac{\overline{I}^2 b^4 3(1-\mu^2)}{E\rho h^4 H^2}$
$\overline{I}$	initial impulse per unit area
K_1,K_2	radial and circumferential changes in curvatures
L	length of the cylinder
m,n	number of axial half-waves and circumferential waves, respectively
q(x,y,t)	radial loading applied to the surface of the cylinder
r	horizontal coordinate of conical shell (fig. 7a)
R	radius of the shell
t	time
u,v,w	displacements of a point on the median surface of the shell (see figs. 1, 7a, and 7b)
w_o	displacement constant, see equation (14)
x,y,z	shell coordinates (see fig. 1)
V	nondimensional strain energy of the shell
α	colatitude coordinate for spherical shell (fig. 7b)

β half opening angle for spherical shell (fig. 7b)

γ,δ,ϵ nonlinearity parameters

ϵ_1,ϵ_2 radial and circumferential extensional strains

$\zeta_c(\tau),\zeta_s(\tau)$ nondimensional generalized coordinates associated with A_n and B_n, respectively

λ shell parameter, $\sqrt{\frac{H}{h}}\left[48(1-\mu^2)\right]^{1/4}$

μ Poisson's ratio

ξ aspect ratio of the vibration mode, $\frac{\pi R/n}{L/m}$

ρ mass density

σ_1,σ_2 radial and circumferential stresses

τ nondimensional time, $\omega_s t$

ω vibration frequency

ω_s calculated linear vibration frequency defined by

$$\left\{\frac{E}{\rho R^2}\left[\frac{\xi^4}{(\xi^2+1)^2}+\frac{\epsilon(\xi^2+1)^2}{12(1-\mu^2)}\right]\right\}^{1/2}$$

ω_L experimental linear vibration frequency

Ω nondimensional frequency, $\frac{\omega}{\omega_s}$

∇^4 biharmonic operator, $\left(\frac{\partial^4}{\partial x^4}+2\frac{\partial^4}{\partial x^2\partial y^2}+\frac{\partial^4}{\partial y^4}\right)$

NONLINEAR FLEXURAL VIBRATIONS OF THIN-WALLED CIRCULAR CYLINDERS

The nonlinear flexural vibrations of thin-walled circular cylinders are analyzed by assuming two vibration modes and applying Galerkin's procedure on the equations of motion. The assumed shape for the radial deflection w and the related stress function F are chosen such that they approximately satisfy the boundary conditions of a cylinder having "freely-supported" ends. In-plane inertia terms are neglected, and a linear stress-strain law is assumed. The nonlinearities in the problem arise from including nonlinear rotation terms in the strain-displacement relations.

Governing Equations

Using the well-known approximations of Donnell's shallow-shell theory as exemplified in reference 3, the equations of motion of a thin-walled circular cylinder can be combined to give

$$D\nabla^4 w + \rho h \frac{\partial^2 w}{\partial t^2} = q + \frac{1}{R}\frac{\partial^2 F}{\partial x^2} + \left[\frac{\partial^2 F}{\partial y^2}\frac{\partial^2 w}{\partial x^2} - 2\frac{\partial^2 F}{\partial x\,\partial y}\frac{\partial^2 w}{\partial x\,\partial y} + \frac{\partial^2 F}{\partial x^2}\frac{\partial^2 w}{\partial y^2}\right] \tag{1}$$

and

$$\frac{1}{Eh}\nabla^4 F = -\frac{1}{R}\frac{\partial^2 w}{\partial x^2} + \left[\left(\frac{\partial^2 w}{\partial x\,\partial y}\right)^2 - \frac{\partial^2 w}{\partial x^2}\frac{\partial^2 w}{\partial y^2}\right] \tag{2}$$

where w is the radial deflection and F is the usual stress function. (The coordinate system and shell geometry are shown in fig. 1.)

Approximate solutions to equations (1) and (2) were obtained by using the following two-mode approximation for the radial deflection:

$$w(x,y,t) = \left\{A_n(t)\cos\frac{ny}{R} + B_n(t)\sin\frac{ny}{R}\right\}\sin\frac{m\pi x}{L}$$
$$+ \frac{n^2}{4R}\left[A_n^2(t) + B_n^2(t)\right]\sin^2\frac{m\pi x}{L} \qquad (n \geq 2) \qquad (3)$$

Here $\cos\frac{ny}{R}\sin\frac{m\pi x}{L}$ and $\sin\frac{ny}{R}\sin\frac{m\pi x}{L}$ are the linear vibration modes of the cylinder, and equation (3) is limited to $n \geq 2$ since only flexural motions are being considered. The bracketed term in (3) is included to satisfy the periodic continuity condition on the circumferential displacement v.

Substitution of equation (3) into the compatibility equation (2) allowed the latter to be solved for F. The expressions for w and F were then examined and found to satisfy the following boundary conditions:

(a) The displacements u, v, and w, and their derivatives satisfy periodicity conditions of the form

$$v(x,y,t) = v(x,y + 2\pi R,t)$$

(b) The radial displacement w goes to zero at the ends of the cylinder, i.e., at $x = 0$ and $x = L$.

(c) To a first approximation, the in-plane stress-resultant N_x, the moment-resultant M_x, and the tangential displacement v all vanish at $x = 0$ and $x = L$. In other words, the coefficients of the linear terms in the expressions for N_x, M_x, and v go to zero at the ends of the cylinder, but the nonlinear terms involving A_n^2, A_nB_n, and B_n^2 do not vanish there. These end conditions are similar to the boundary conditions for a cylinder which has freely-supported ends.

The applied loading, $q(x,y,t)$, was chosen such that only one mode is directly excited:

$$q(x,y,t) = Q_{mn} \cos \frac{ny}{R} \sin \frac{m\pi x}{L} \cos \omega t \tag{4}$$

Finally, the expressions for w, F, and q were substituted into equation (1) and a Galerkin procedure was used to obtain two nonlinear differential equations for the modal amplitudes A_n and B_n. In nondimensional form, these coupled equations are

$$\frac{d^2\zeta_c}{d\tau^2} + \zeta_c + \frac{3\epsilon}{8}\zeta_c\left[\zeta_c \frac{d^2\zeta_c}{d\tau^2} + \left(\frac{d\zeta_c}{d\tau}\right)^2 + \zeta_s \frac{d^2\zeta_s}{d\tau^2} + \left(\frac{d\zeta_s}{d\tau}\right)^2\right]$$
$$- \epsilon\gamma\zeta_c\left(\zeta_c^2 + \zeta_s^2\right) + \epsilon^2\delta\zeta_c\left(\zeta_c^2 + \zeta_s^2\right)^2 = G_{mn} \cos \Omega\tau \tag{5a}$$

and

$$\frac{d^2\zeta_s}{d\tau^2} + \zeta_s + \frac{3\epsilon}{8}\zeta_s\left[\zeta_s \frac{d^2\zeta_s}{d\tau^2} + \left(\frac{d\zeta_s}{d\tau}\right)^2 + \zeta_c \frac{d^2\zeta_c}{d\tau^2} + \left(\frac{d\zeta_c}{d\tau}\right)\right]^2$$
$$- \epsilon\gamma\zeta_s\left(\zeta_s^2 + \zeta_c^2\right) + \epsilon^2\delta\zeta_s\left(\zeta_s^2 + \zeta_c^2\right)^2 = 0 \tag{5b}$$

where the nondimensional variables are

$$\zeta_c = \frac{A_n}{h} \qquad \zeta_s = \frac{B_n}{h}$$

$$\tau = \omega_s t \qquad G_{mn} = \frac{Q_{mn}}{\rho h^2 \omega_s^2}$$

the nondimensional frequency is

$$\Omega = \frac{\omega}{\omega_s}$$

and the nonlinearity parameters are

$$\epsilon = \left(\frac{n^2 h}{R}\right)^2$$

$$\gamma = \frac{\xi^4\left[\frac{1}{(\xi^2+1)^2} - \frac{1}{16} - \frac{\epsilon}{12(1-\mu^2)}\right]}{\left[\frac{\xi^4}{(\xi^2+1)^2} + \frac{\epsilon(\xi^2+1)^2}{12(1-\mu^2)}\right]}$$

and

$$\delta = \frac{3\xi^4}{16}\frac{\left[\frac{1}{(\xi^2+1)^2} + \frac{1}{(9\xi^2+1)^2}\right]}{\left[\frac{\xi^4}{(\xi^2+1)^2} + \frac{\epsilon(\xi^2+1)^2}{12(1-\mu^2)}\right]}$$

In these expressions, the parameter ξ represents the aspect ratio of the vibration mode:

$$\xi = \frac{\pi R/n}{L/m} = \frac{\text{Circumferential wavelength}}{\text{Axial wavelength}} \tag{6}$$

Examination of the expressions for γ, δ, ϵ, and ξ in equations (5) and (6) leads to the following observations:

(a) As the length of the cylinder tends to infinity, the parameters ξ, γ, and δ all tend to zero, and equations (5) approach the previous results for rings (ref. 1).

(b) Each of the nonlinear terms in equation (5) is multiplied by ϵ; consequently, ϵ can be viewed as the basic nonlinearity parameter in the problem. Linear vibrations occur for $\epsilon = 0$, and increasing ϵ makes the vibrations increasingly nonlinear.

Approximate Solutions by the Method of Averaging

Equations (5) can be solved approximately by use of the method of Krylov-Bogoliubov, often called "The Method of Averaging." Such solutions will be

presented for vibrations involving (a) only the driven mode and (b) both the driven mode and its companion mode. In the discussion which follows, the term "driven mode" relates to $\zeta_c(\tau)$ and cos ny/R sin mπx/L; the term "companion mode" refers to $\zeta_s(\tau)$ and sin ny/R sin mπx/L.

Response of a single bending mode.- Since the applied loading (eq. (4)) directly drives only one mode of the cylinder, a possible solution to equations (5) involves the response of only the driven mode. Application of the method of averaging for this case gives

$$\left.\begin{aligned} \zeta_c(\tau) &= \bar{A} \cos \Omega\tau \\ \zeta_s(\tau) &= 0 \end{aligned}\right\} \tag{7}$$

where $\bar{A}$ can be computed from

$$(1 - \Omega^2)\bar{A} - \frac{3\epsilon}{16}\Omega^2\bar{A}^3 - \frac{3\epsilon\gamma}{4}\bar{A}^3 + \frac{5}{8}\epsilon^2\delta\bar{A}^5 = G_{mn} \tag{8}$$

Equation (8) can be used to compute the variation of $\bar{A}$ with Ω for given values of ϵ, γ, δ, and G_{mn}. When G_{mn} is nonzero, the forced vibration response of a single mode is obtained; the case of free nonlinear vibrations results when G_{mn} is put equal to zero.

Stability of the one-mode response.- The stability of the preceding solution was investigated by perturbing $\zeta_c(\tau)$ and $\zeta_s(\tau)$. A study of the resulting Mathieu-Hill equations indicated that within terms of order ϵ^2

(1) Perturbations of ζ_c are unstable within the area bounded by

$$1 - \frac{9\epsilon A^2}{8}\left(\gamma + \frac{1}{4}\right) < \Omega < 1 - \frac{3\epsilon\bar{A}^2}{8}\left(\gamma + \frac{1}{4}\right)$$

(2) Perturbations of ζ_s are unstable within the region

$$1 - \frac{3\epsilon\bar{A}^2}{8}\left(\gamma + \frac{1}{4}\right) < \Omega < 1 + \frac{\epsilon\bar{A}^2}{8}\left(\frac{3}{4} - \gamma\right)$$

(3) Both types of perturbations are unstable in narrow regions near $\Omega = 1/2, 1/3, \ldots$

The first instability region coincides with the locus of vertical tangents to the response curves and indicates the well-known jump phenomena. The narrow areas near $\Omega = 1/2, 1/3, \ldots$, denote possible ultraharmonic responses. The remaining region, (2), indicates the area in which the companion mode is parametrically unstable due to nonlinear coupling with the driven mode. To obtain adequate solutions in region (2), it is necessary to consider motions where both modes vibrate.

Response of the coupled bending modes.- When $\zeta_s(\tau)$ and $\zeta_c(\tau)$ both oscillate, the method of averaging gives the approximate solution

$$\left.\begin{aligned} \zeta_c(\tau) &= \bar{A} \cos \Omega\tau \\ \zeta_s(\tau) &= \bar{B} \sin \Omega\tau \end{aligned}\right\} \tag{9}$$

where $\bar{A}$ and $\bar{B}$ satisfy the following equations:

$$(1 - \Omega^2)\bar{A} + \frac{3\epsilon\Omega^2}{16}\bar{A}(\bar{B}^2 - \bar{A}^2) - \frac{\epsilon\gamma\bar{A}}{4}(3\bar{A}^2 + \bar{B}^2) + \frac{\epsilon^2\delta}{8}\bar{A}\left(5\bar{A}^4 + 2\bar{A}^2\bar{B}^2 + \bar{B}^4\right) = G_{mn} \tag{10a}$$

$$\left(1 - \Omega^2\right)\bar{B} + \frac{3\epsilon\Omega^2}{16}\bar{B}\left(\bar{A}^2 - \bar{B}^2\right) - \frac{\epsilon\gamma\bar{B}}{4}\left(3\bar{B}^2 + \bar{A}^2\right) + \frac{\epsilon^2\delta}{8}\bar{B}\left(5\bar{B}^4 + 2\bar{A}^2\bar{B}^2 + \bar{A}^4\right) = 0 \tag{10b}$$

If $\bar{B} = 0$, equations (9) and (10) revert to the single mode case discussed previously. When $\bar{B}$ is not zero, the variation of $\bar{A}$ and $\bar{B}$ with Ω can be

computed by solving equations (10a) and (10b) simultaneously, for given values of ϵ, γ, δ, and G_{mn}.

DISCUSSION OF THE CYLINDER RESULTS

Figure 2 illustrates the response curves for both free and forced vibrations of a single bending mode. The dashed curve represents free nonlinear vibrations and was obtained from equation (8) with G_{mn} put equal to zero. The forced vibration response is given by the solid lines, which were computed from equation (8) for $G_{mn} = 0.1$. Both the free and forced response curves demonstrate a slight nonlinearity of the softening type. The value of ϵ used in these calculations was 0.01, and the values of γ and δ which were used correspond to $\xi = 0.1$, $\epsilon = 0.01$, and $\mu = 0.3$. These values of ξ and ϵ are representative of a cylinder that is vibrating in the $m = 1$, $n = 10$ mode and which has a length/radius of π and a radius/thickness ratio of 1000. The slight nonlinearity shown in figure 2 is typical of cylinders that are relatively long and thin-walled. For other modes and geometries, however, the nonlinearity can be much more pronounced.

This result is indicated in figures 3 and 4, which show how variations in the parameters ϵ and ξ affect the nonlinearity of the vibrations. Figure 3 shows several free vibration response curves computed from equation (8) for $G_{mn} = 0$ and for five values of ϵ ranging from 0 to 1.0. The solid lines were calculated for values of γ and δ corresponding to an aspect ratio $\xi = 1/2$, and the dashed curves are for $\xi = 2$. Both sets of curves in figure 3 demonstrate that the strength of the nonlinearity is determined primarily by the parameter $\epsilon = \left(\frac{n^2 h}{R}\right)^2$. The nonlinearity is generally small for

vibrations involving very thin cylinders and/or low circumferential mode numbers, n. Conversely, strong nonlinearities occur for the case of thick cylinders and/or high circumferential mode numbers.

The character of the nonlinearity (i.e., whether it is softening or hardening) depends primarily on ξ, which is the aspect ratio of the vibration mode. This result is illustrated in figure 4, which shows several free vibration response curves computed from equation (8) for values of ξ ranging from 0.10 to 4.0. The solid lines show the results of the present analysis; they were calculated for constant values of the nonlinearity parameter $\epsilon = 1.0$ and Poisson's ratio $\mu = 0.3$. The present calculations show that the vibrations are generally of the softening type when the aspect ratio ξ is less than unity. For larger values of the aspect ratio, the solid curves indicate a nonlinearity of the hardening type.

For comparison purposes, the dashed curves in figure 4 illustrate Chu's results (ref. 4), which correspond to $\epsilon = 1.0$ and $\mu = 0.318$. Chu points out that his results possess a symmetric dependence on the aspect ratio parameter, whereby his curves for $\xi = 1/2, 1/4, 1/8 \ldots$ coincide with those for $\xi = 2, 4, 8 \ldots$, respectively. Such a symmetric dependence on the aspect ratio seems to conflict with the basic geometric nonsymmetry of the problem - i.e., the surface of the cylinder is curved in the circumferential direction but not in the axial direction.

With regard to this point, it will be noted that the present results do not exhibit a symmetric dependence on the aspect ratio and do not agree with the calculations of ref. 4. The major reason that the previous studies (refs. 3 and 4) do not agree with the present work appears to be that the former do not satisfy the necessary geometric continuity constraint on the

circumferential displacement, v. (The available experiments tend to favor the present analysis; they will be discussed shortly.)

The previous studies did not consider coupled mode responses involving both a driven mode and its companion. The solid lines shown in figure 5 illustrate such a coupled mode response for a typical cylinder. The response curves were calculated from equations (10a) and (10b) with $\epsilon = 0.01$, $G_{mn} = 0.1$, and γ and δ corresponding to $\xi = 0.1$. It is of interest to note that the solid response curves are analogous to the results obtained for nonlinear vibrations of rings and for nonlinear vibration absorbers (refs. 1 and 5.)

Along the a-b portion of the solid curves (fig. 5), $\bar{B}$ is zero and only the driven mode responds. Along the segments b-c-d and e-f-g, both the driven mode and its companion respond with comparable amplitudes; in this case, the response curves are adjacent to the dashed lines, o-n. The response curves exhibit vertical tangents at points c, f, g, and h, and the segments c-d and f-g are suspected of being unstable. Along g-h-i-j, the response of the companion mode is much greater than that of the driven mode. This situation is analogous to the vibration absorber response in which the driven mass experiences very little motion while the absorber mass vibrates with large displacements. For ring vibrations, the segment corresponding to g-h-i-j was found to be unstable, and a similar result appears true for cylinders. To the left of point g, the vibrations apparently revert to the one mode case, with $\bar{B} = 0$ and $\bar{A}$ given by equation (8). For some cylinders, this may result in a "gap" region, in which both solutions (7) and (9) are unstable. Such unstable gaps in the response have been observed in related problems, and analog computer

studies indicate that nonsteady vibrations with rapidly changing amplitudes occur in these regions. (See refs. 1, 6, and 7 in this regard.)

Experimental results for the nonlinear flexural vibrations of thin-walled circular cylinders are rather scarce. Among the best available data is that of Olson (ref. 2) who obtained nonlinear forced response curves for the vibration of a thin cylindrical shell. Olson's experimental data is shown by the circles and dashed lines in figure 6. The solid line in figure 6 is the free vibration response curve calculated from equation (8) for $G_{mn} = 0$ and with values of ϵ, γ, and δ that correspond to Olson's experiment. Both theory and experiment indicate a nonlinearity of the softening type for this case, whereas the previous theoretical results (refs. 3 and 4) indicate a hardening type of nonlinearity for all cylinders. The agreement shown in figure 6 is reasonably good, despite the fact that the theory is for freely-supported ends whereas the test cylinders had end clamping. It is of interest to note that Olson also detected nonsteady vibrations in his experiments; these vibrations may have been due to coupled mode responses.

Nonlinear Vibrations of Related Axisymmetric Systems

The results for thin cylindrical shells are qualitatively similar to those for rings; in both cases, the companion mode can be parametrically excited and participate in the motion. In some cases, the driven mode and its companion combine to produce a circumferentially travelling wave; responses of this type have been detected for rings (ref. 1), cylindrical shells (ref. 8), conical shells (ref. 9), and circular plates (ref. 10). It seems reasonable to expect that similar motions will occur for the nonlinear vibration of other flexible axisymmetric bodies. This suggests the possibility of formulating a general

theory for the nonlinear vibration of axisymmetric systems, and the present work is being extended along these lines.

DYNAMIC SNAP-THROUGH BUCKLING OF ELASTIC SHALLOW CONICAL AND SPHERICAL CAPS

A second class of nonlinear problems which has been studied involves the axisymmetric snap-through buckling of shallow conical and spherical caps subjected to uniformly distributed impulsive loads. For this problem, it is assumed that the duration of the impulse is short with respect to the period of the fundamental flexural mode, but long with respect to the first extensional mode of the shell. The shell is assumed to behave as a single-degree-of-freedom system during its first cycle of oscillation and inplane inertia is neglected.

The method of attack is to investigate the behavior of the shell at the time when its amplitude reaches a maximum. Treating the shell as an undamped single-degree-of-freedom system, the internal strain energy at maximum displacement is equal to the initial kinetic energy of the shell. The initial kinetic energy can in turn be related to the applied impulse by considering conservation of momentum.

Thus, the initial impulse can be obtained as a function of the maximum displacement. The maximum displacement w will increase with increase in initial impulse I until the impulse is sufficient to cause snap-through buckling. At the snap-through impulse there will be a sudden increase in maximum displacement with respect to a change in initial impulse. The condition for snap-through is therefore given by

$$\frac{dw}{dI} = \infty \quad \text{or} \quad \frac{dI}{dw} = 0$$

Conical Shell

The problem to be considered first is that of a shallow conical shell which deforms axisymmetrically. The results will be summarized briefly and further details may be obtained in reference 11. The cone has a height H, an external radius b, and thickness h. The radius to a point on the middle surface is r (see fig. 7a). The shell is considered shallow in the sense that the rise angle of the cone and the sine of the rise angle can be replaced by H/b.

The strain energy of the shell can be expressed as

$$V = \frac{1}{2(1 - \mu^2)H^2} \int_0^b \left(\epsilon_1^2 + \epsilon_2^2 + 2\mu\epsilon_1\epsilon_2\right)r\,dr + \frac{2}{\lambda^4} \int_0^b \left(K_1^2 + K_2^2 + 2\mu K_1 K_2\right)r\,dr \tag{11}$$

where the factor $2\pi H^2 Eh$ has been used to render the strain energy nondimensional. Here ϵ_1, ϵ_2 and K_1, K_2 are, respectively, the extensional strains and curvatures in the radial and circumferential directions. Young's modulus is denoted by E and Poisson's ratio by μ; λ is the shell parameter, which is defined by

$$\lambda^2 = \frac{H}{h}\sqrt{48(1 - \mu^2)} \tag{12}$$

The nonlinear strains and curvatures given in equation (11) are related to the displacements by

$$\left.\begin{aligned} \epsilon_1 &= \frac{du}{dr} + \frac{H}{b}\frac{dw}{dr} + \frac{1}{2}\left(\frac{dw}{dr}\right)^2 & \qquad K_1 &= \frac{d^2w}{dr^2} \\ \epsilon_2 &= \frac{u}{r} & \qquad K_2 &= \frac{1}{r}\frac{dw}{dr} \end{aligned}\right\} \tag{13}$$

where u and w are the maximum deflections in the horizontal (r) and vertical (z) directions, respectively.

Solutions for Various Boundary Conditions

Consider first the solution for the conical cap which has boundary conditions at $r = b$ such that the displacement is restrained in the radial direction (i.e., $u = 0$). The shell can be either clamped or simply-supported with respect to the w displacement at the boundary.

The maximum deflection can be approximated by

$$w = w_o H\left(1 - \frac{r^2}{b^2}\right)\left(1 - C\,\frac{r^2}{b^2}\right) \tag{14}$$

where w_o and C are constants. The boundary conditions at $r = b$ can be satisfied by a proper choice of C, that is,

Clamped: $\quad \frac{dw}{dr} = 0, \quad C = 1$

Simply supported: $\quad M_1 = -D(K_1 + \mu K_2) = 0, \quad C = \frac{1 + \mu}{5 + \mu}$

The shape given by equation (14) corresponds to the deflection of a circular plate subjected to a uniform lateral load and supported at the boundary.

Following the procedure just outlined leads to an equation such as the following one which holds for the clamped restrained boundary conditions $\left(\text{i.e., } \left.\frac{dw}{dr}\right|_{r=b} = u\Big|_{r=b} = 0\right)$.

$$I = \lambda^4\left[0.0288{w_o}^4 - 0.0908{w_o}^3 + {w_o}^2\left(0.0719 + \frac{5.3333}{\lambda^4}\right)\right] \tag{15}$$

where

$$I = \frac{\bar{I}^2 b^4 3(1 - \mu^2)}{Eh^4 H^2} \tag{16}$$

$\bar{I}$ is the initial uniformly distributed impulse per unit area, ρ is the mass density of the shell, and value of $\mu = 0.3$ has been used.

The condition for snap-through is $dI/dw_o = 0$ which gives the critical deflection for the clamped case as

$$w_o = 1.1823 - \sqrt{0.1496 - \frac{92.5926}{\lambda^4}} \tag{17}$$

Note that at certain values of λ the amplitude w_o becomes imaginary; at these points there is no real w_o corresponding to the snap-through condition. The physical interpretation of imaginary values of w_o is that the shell does not exhibit a snapping phenomenon and instead the motion is smooth and oscillatory. The minimum values for λ for the clamped case corresponding to real w_o is $\lambda_{min} = 5.0$. Thus, for example, in the case of a cone with a clamped restrained boundary, snap-through buckling does not occur unless λ exceeds 5.0 which happens when the rise of the cone H exceeds $3.78h$.

A plot of the impulse required for snap-through as a function of the shell parameter λ is presented in figure 8. These curves are obtained from equation (15) taking account of equation (17). Similar calculations were carried out for all combinations of simply-supported or clamped and restrained (i.e., radial displacement $u = 0$) or unrestrained (i.e., radial stress $\sigma_1 = 0$) boundary conditions. These are also given in figure 8.

A study of the magnitude of critical deflection occurring at snap-through indicates that it is of the order of the rise of the cone. For example, when $\lambda = 6.0$, $\frac{w_o}{H} = 0.902$ for the clamped restrained case.

Spherical Cap Results

Results were also obtained for the snap-through buckling of a spherical cap having the same boundary conditions and loading as the cone. The appropriate strain-displacement relations were taken as

$$\left.\begin{aligned} \epsilon_1 &= \frac{1}{R}\left(\frac{du}{d\alpha} - w\right) + \frac{1}{2R^2}\left(\frac{dw}{d\alpha}\right)^2 \\ \epsilon_2 &= \frac{1}{R}\left(\frac{u}{\alpha} - w\right) \\ K_1 &= \frac{1}{R^2}\frac{d^2w}{d\alpha^2} \\ K_2 &= \frac{1}{R^2}\frac{1}{\alpha}\frac{dw}{d\alpha} \end{aligned}\right\} \tag{18}$$

Here α is the opening angle variable and R is the radius of the sphere (fig. 7b). The quantities u and w are the tangential and normal displacements of the shell.

The displacement w is taken in the same form as equation (14) and the procedure for the spherical cap is directly analogous to that for the conical cap. A plot of the impulse required for snap-through as a function of shell parameter λ is given in figure 9 for boundary conditions comparable to those of the cone, i.e., simply-supported and clamped, restrained and unrestrained. The results for the clamped restrained spherical cap agree identically with those given in reference 12.

Discussion of Results

It is interesting to note in figure 8 that for relatively large values of λ the strength of the simply-supported restrained conical shell is greater

than the comparable fixed case. On the other hand for small values of λ where the rise of the cone is quite small, the reverse is true.

The first effect has been noted previously by Humphreys and Bodner (ref. 12) for dynamic buckling of a long cylindrical panel. They found that for all ranges of the curvature parameter the simply-supported panel exhibited a greater resistance to snap-through than did clamped panels.

The results for the spherical cap in figure 9 follow the same trend with the simply-supported shell always being stronger with respect to dynamic buckling than the clamped shell. These results emphasize the importance of boundary conditions in assessing the dynamic strength of this class of shells.

It is also of interest to compare the behavior of a shallow conical shell with that of a shallow spherical shell of comparable geometry and boundary conditions. Since a shallow sphere cannot be compared directly with a shallow cone, two comparisons were made, first with equal rises and the second with equal edge slopes. Both results are plotted in figure 10 for the restrained boundary conditions where the spherical cap parameters have been used as a basis for the plots. In general, figure 10 shows that for a conical or spherical shell of the same rise H, the stronger structure to resist dynamic buckling is the sphere. Figure 10 also indicates that if the cone and sphere have the same slope at the boundary, the sphere is not as strong as the cone. The same qualitative results were also found to hold for the unrestrained cases. This suggests that a shallow conical cap with a dynamic buckling impulse equivalent to that of a spherical cap has a height larger than the sphere.

A final comment should be made with respect to the accuracy of the present analysis. The two major sources of error in the analysis lie in the assumption that the shell behaves as a single-degree-of-freedom system and the requirement

that the shell deform axisymmetrically. Both of these effects become more important with increasing shell rise. References 13 and 14 present results for the axisymmetric dynamic snap-through buckling of a clamped spherical cap using five degrees of freedom. The results are shown in figure 9 as the dotted line. In general good correlation is obtained for the single degree of freedom up to λ of about 7. Some disagreement between the present results and those of reference 14 occurs for the cutoff point; however, this may be attributed to the difficulty in defining a finite cutoff point in the method used by reference 14.

Results for the axisymmetric static buckling of a clamped spherical cap are known to be adequate up to λ of about 5.5 with nonsymmetric effects predominating for larger values of λ. Since the dynamic snap-through requires a certain amount of time to occur, it seems reasonable to expect that axisymmetric behavior will hold in the dynamic case up to a higher λ than for static snap-through. In view of these effects the results given herein are felt to be inadequate for λ beyond about nine for conical shells and for λ beyond seven for spherical shells.

CONCLUDING REMARKS

A solution has been given for the nonlinear flexural vibrations of a thin-walled circular cylinder subjected to harmonic excitation of a single mode. It was found that for certain frequencies of the driving force, only the driven mode responded. For other frequencies, however, the companion mode also became excited due to nonlinear parametric coupling between the modes. Results given indicate that the nonlinearity for a cylindrical shell can be either of the softening or hardening type depending on the aspect ratio of the vibration mode.

This conclusion differs from the results of Chu which indicated that the nonlinearity was always of the hardening type. The available experimental data agrees reasonably well with the analysis presented here. A discussion is also given which relates the present study to the nonlinear vibrations of other axisymmetric systems.

Results are also given for the snap-through buckling of shallow conical and spherical caps subjected to a uniformly distributed idealized impulse. Solutions are given for a variety of boundary conditions for both types of shells and several comparisons are made between the results. One comparison shows that for conical caps a simply-supported shell can resist a larger impulse than a clamped cone. Another comparison between spherical and conical caps having the same height indicates that the sphere can resist a larger impulse than the cone before buckling.

REFERENCES

1. Evensen, D. A.: Non-Linear Flexural Vibrations of Thin Circular Rings. PhD Thesis, California Institute of Technology, Pasadena, California, 1964.

2. Olson, M. D.: Some Experimental Observations on the Nonlinear Vibrations of Cylindrical Shells. AIAA Journal, Vol. 3, No. 9, Sept. 1965, pp. 1775-1777.

3. Reissner, E.: Non-Linear Effects in the Vibration of Cylindrical Shells. Aeromechanics Report No. 5-6, Ramo-Wooldridge Corporation, 1955.

4. Chu, H.: Influence of Large Amplitudes on Flexural Vibrations of a Thin Circular Cylindrical Shell. Journal of the Aero-Space Sciences, Vol. 28, No. 8, 1961, pp. 602-609.

5. Arnold, F. R.: Steady-State Behavior of Systems Provided With Nonlinear Dynamic Vibration Absorbers. Journal of Applied Mechanics, Vol. 22, Trans. ASME, Vol. 77, 1955, pp. 487-492.

6. Miles, J. W.: Stability of Forced Oscillations of a Spherical Pendulum. Quarterly of Applied Mathematics, Vol. 20, 1962, pp. 21-32.

7. Hutton, R. E.: An Investigation of Resonant, Non-Linear, Non-Planar Free Surface Oscillations of a Fluid. NASA TN D-1870, 1963.

8. Mixson, J. S., and Herr, R. W.: An Investigation of the Vibration Characteristics of Pressurized Thin-Walled Circular Cylinders Partly Filled With Fluid. NASA TR-145, 1962.

9. Mixson, J. S., NASA Langley Research Center: (Private communication.)

10. Tobias, S. A.: Nonlinear Forced Vibrations of Circular Discs. Engineering, Vol. 179, 1958, pp. 51-56.

11. Fulton, Robert E.: Dynamic Axisymmetric Buckling of Shallow Conical Shells Subjected to Impulsive Loads. Journal of Applied Mechanics, March 1965, pp. 129-134.

12. Humphreys, J. S., and Bodner, S. R.: Dynamic Buckling of Shells Under Impulsive Loadings. Proc. ASCE, Vol. 88, EM2, April 1962, pp. 17-36.

13. Radkowski, P. P., Humphreys, J. S., Bodner, S. R., Payton, R. G., and Budiansky, B.: Studies on the Dynamic Response of Shell Structures to Pressure Pulse. AFSWC-TR61-31 (II), AVCO RAD, July 1961.

14. Budiansky, B., and Roth, R. S.: Axisymmetric Dynamic Buckling of Clamped Shallow Spherical Shells. Collected Papers on Instability of Shell Structures - 1962. NASA TN D-1510, December 1962.

15. Huang, Nai-Chien: Unsymmetrical Buckling of Shallow Spherical Shells, AIAA Journal, Vol. 1, No. 4, April 1963, p. 945.

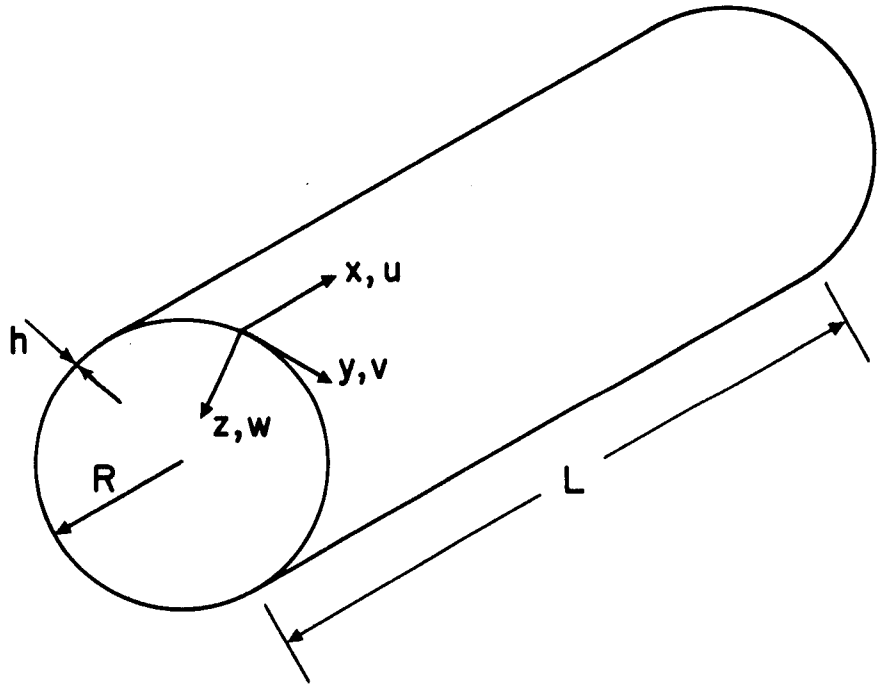

Figure 1.- Shell geometry and coordinate system.

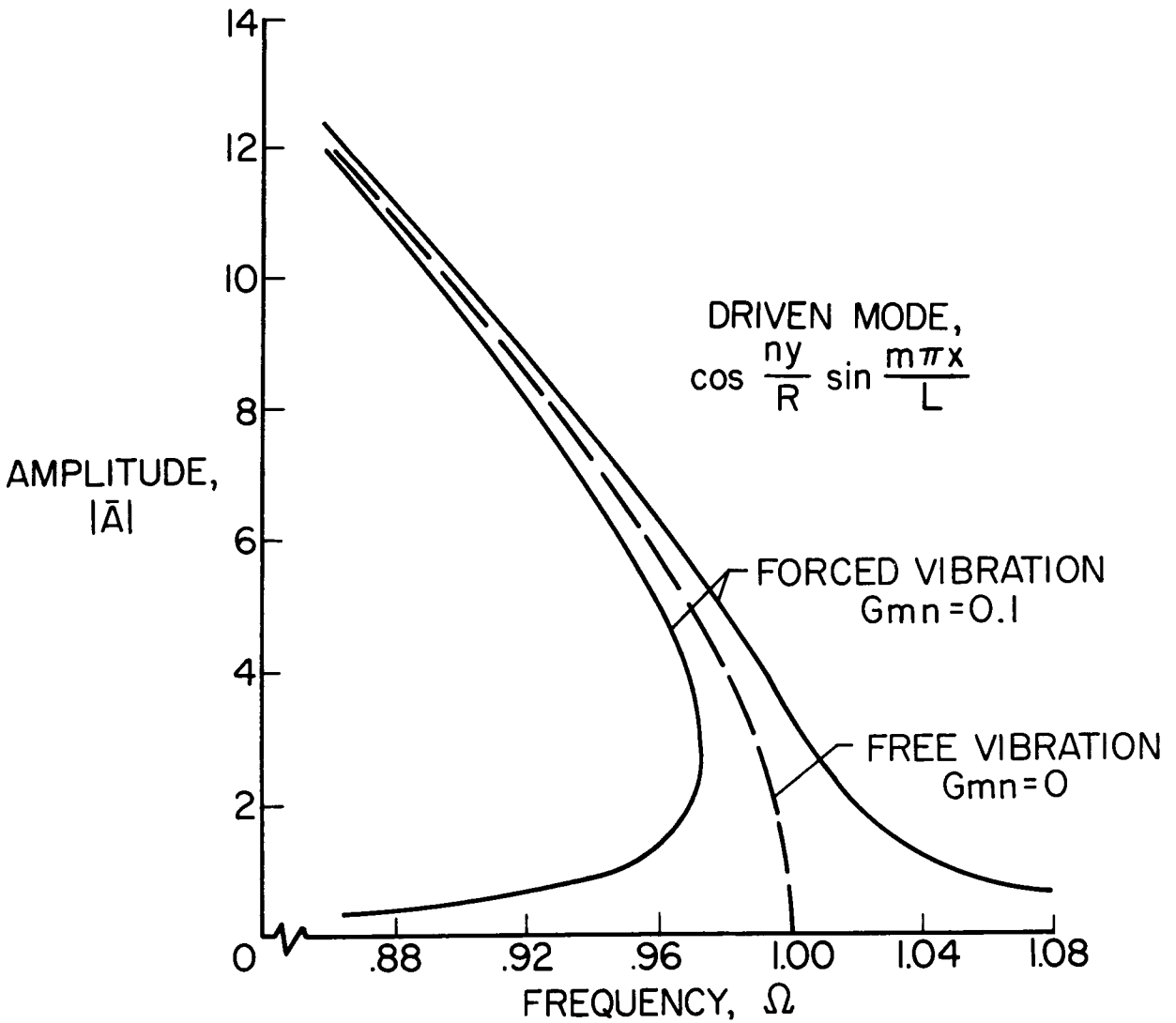

Figure 2.- Single mode response. Forced and free vibrations, $\epsilon = 0.01$, $\xi = 0.1$.

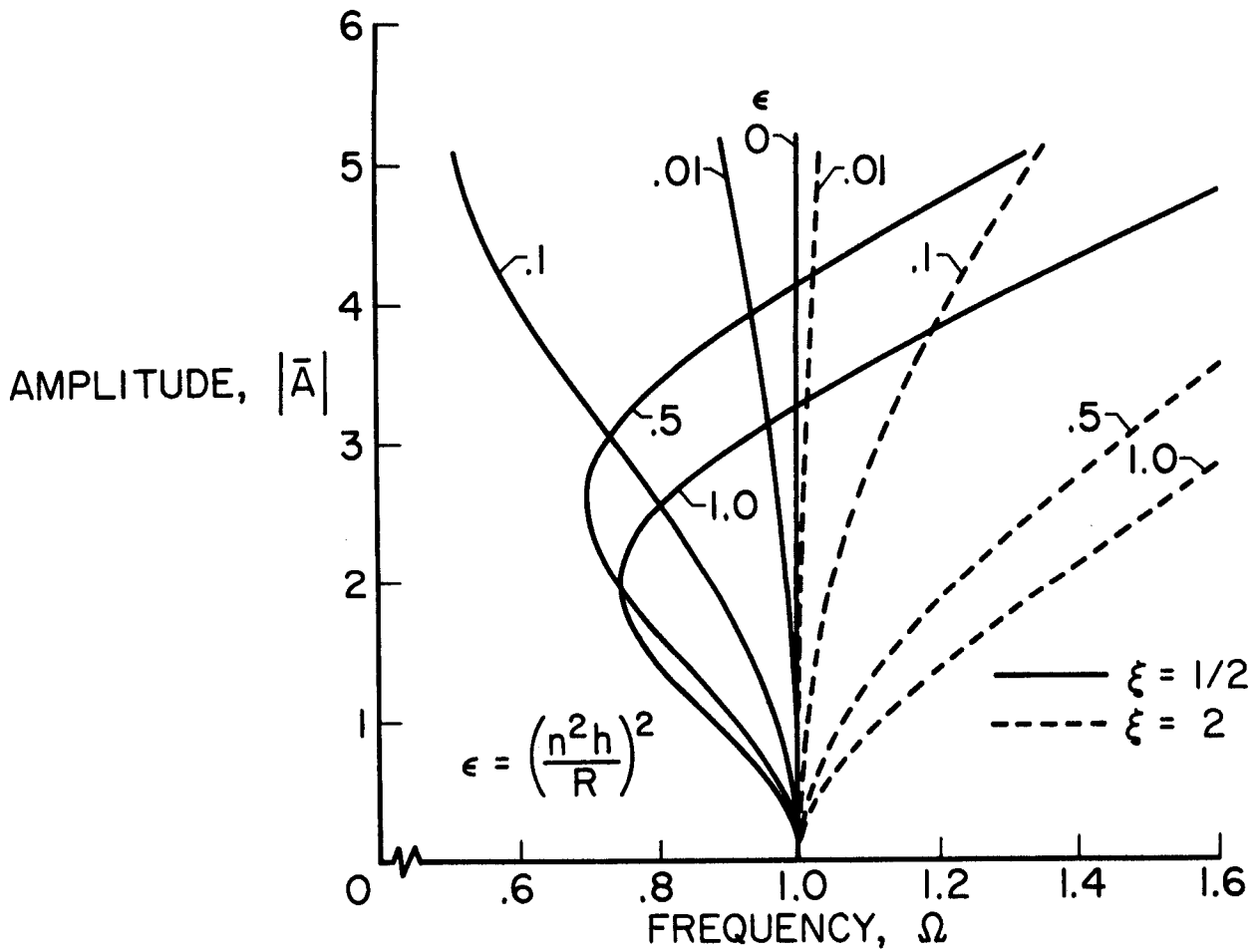

Figure 3.- Influence of large amplitudes on the vibration frequency for various values of ϵ. Free vibrations; one mode; ξ = 1/2 and 2. Poisson's ratio, μ = 0.3.

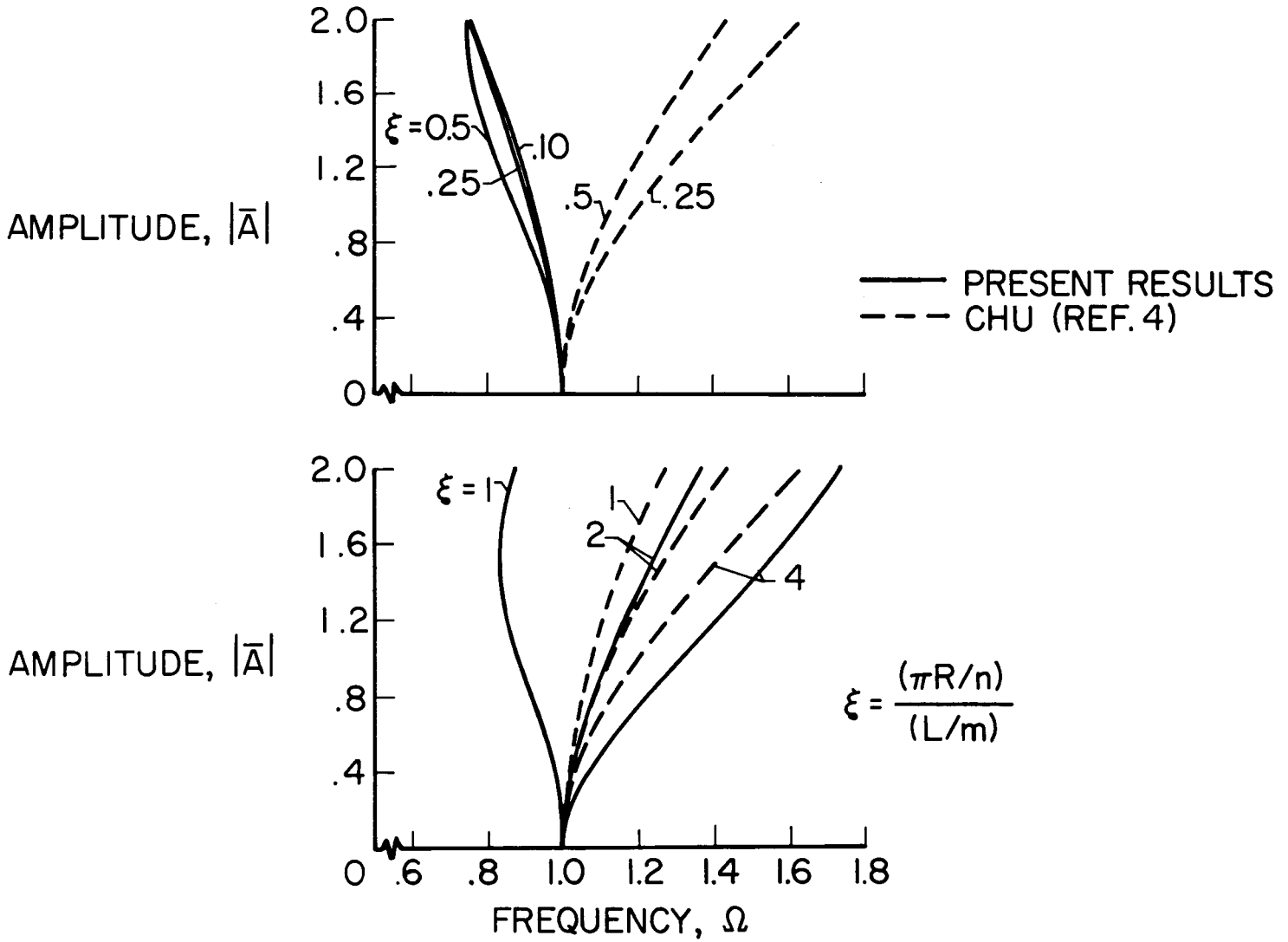

Figure 4.- Influence of large amplitudes on the vibration frequency for various aspect ratios. Free vibrations; one mode; $\epsilon = 1.0$. Poisson's ratio, $\mu = 0.3$.

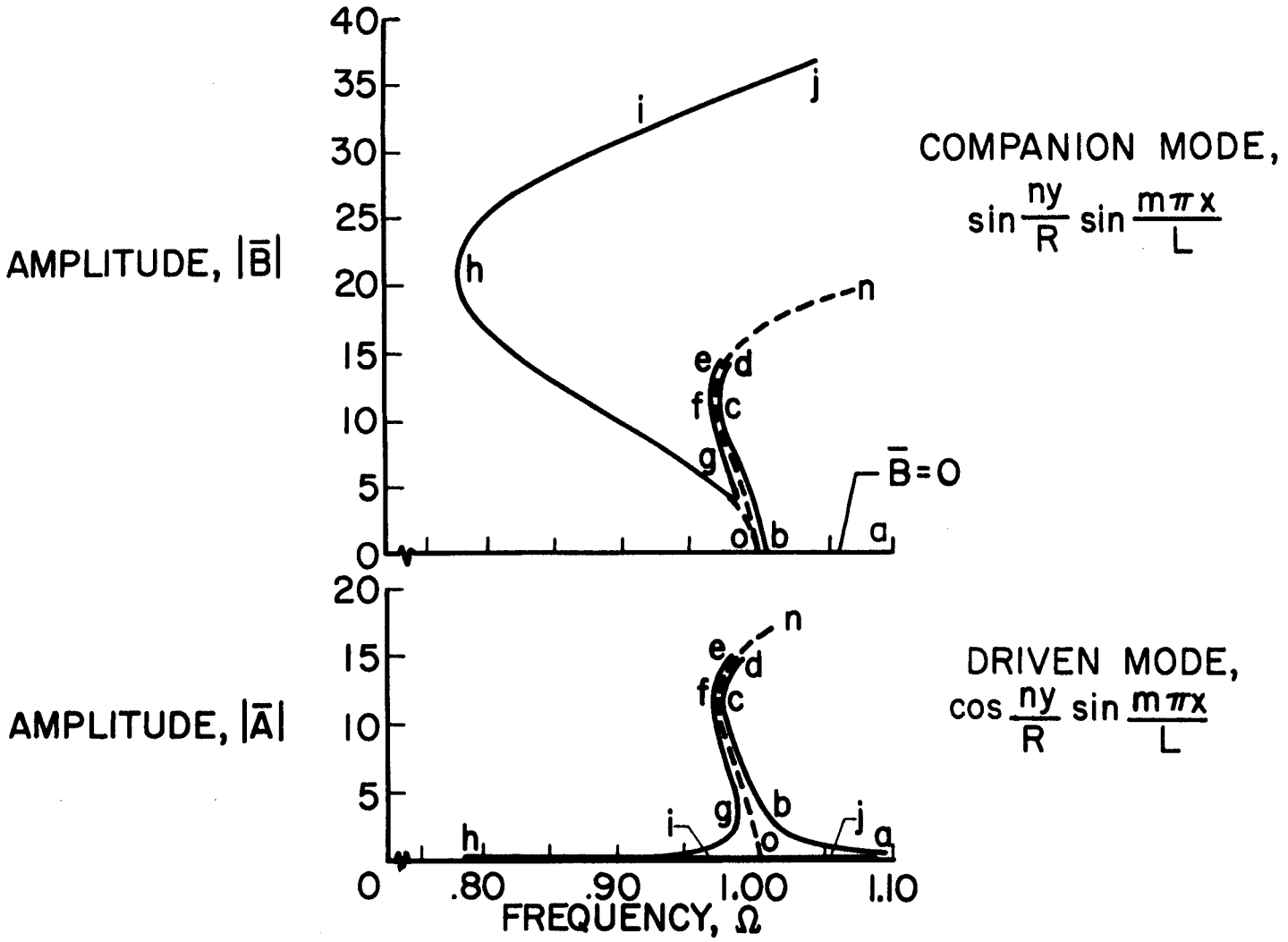

Figure 5.- Coupled-mode response. Forced vibrations; $\epsilon = 0.01$; $\xi = 0.1$; $G_{mn} = 0.1$; $\mu = 0.3$.

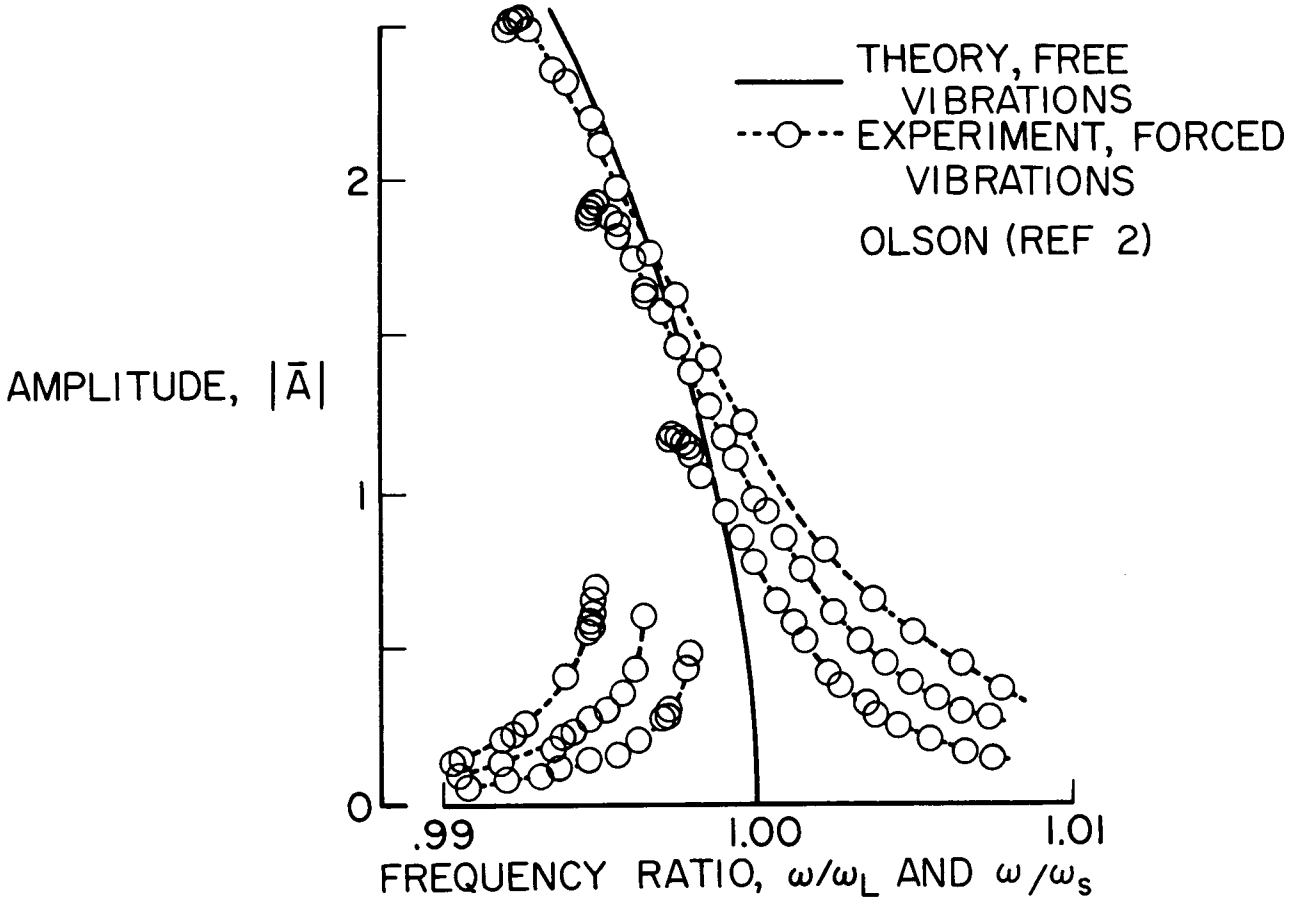

Figure 6.- Comparison with experimental results.

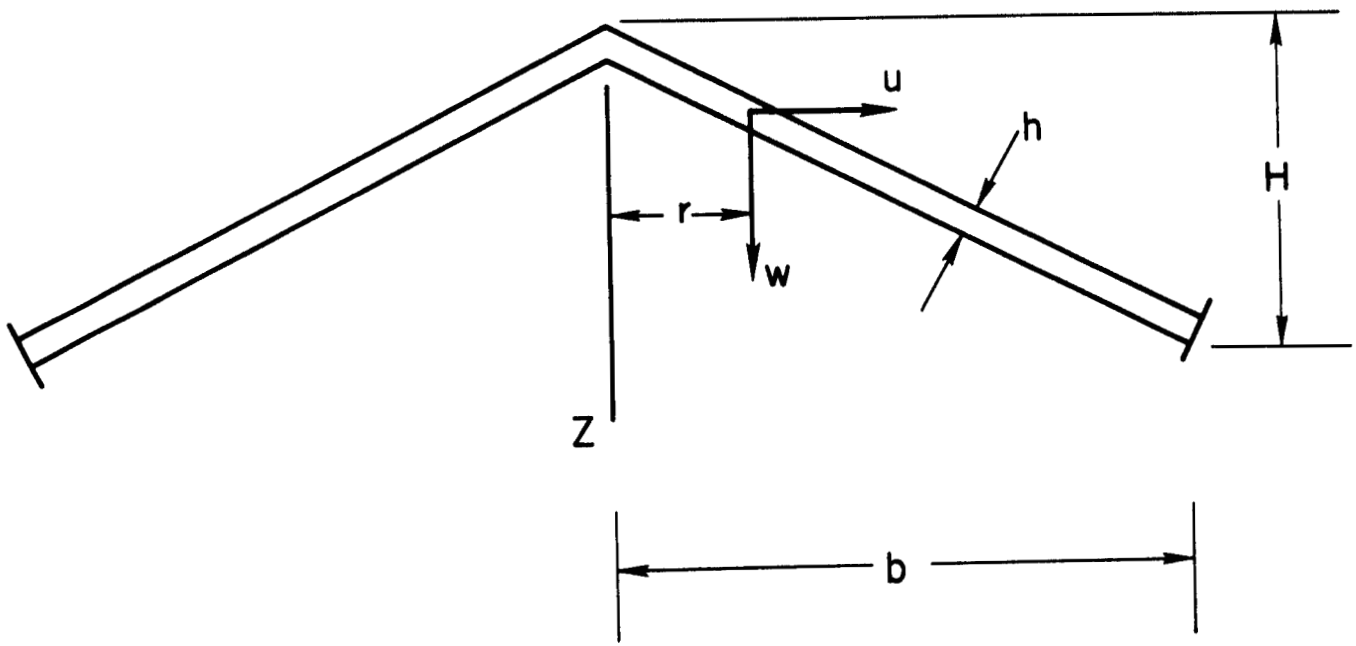

(a) Conical cap.

Figure 7.- Shell geometry for axisymmetric shallow caps.

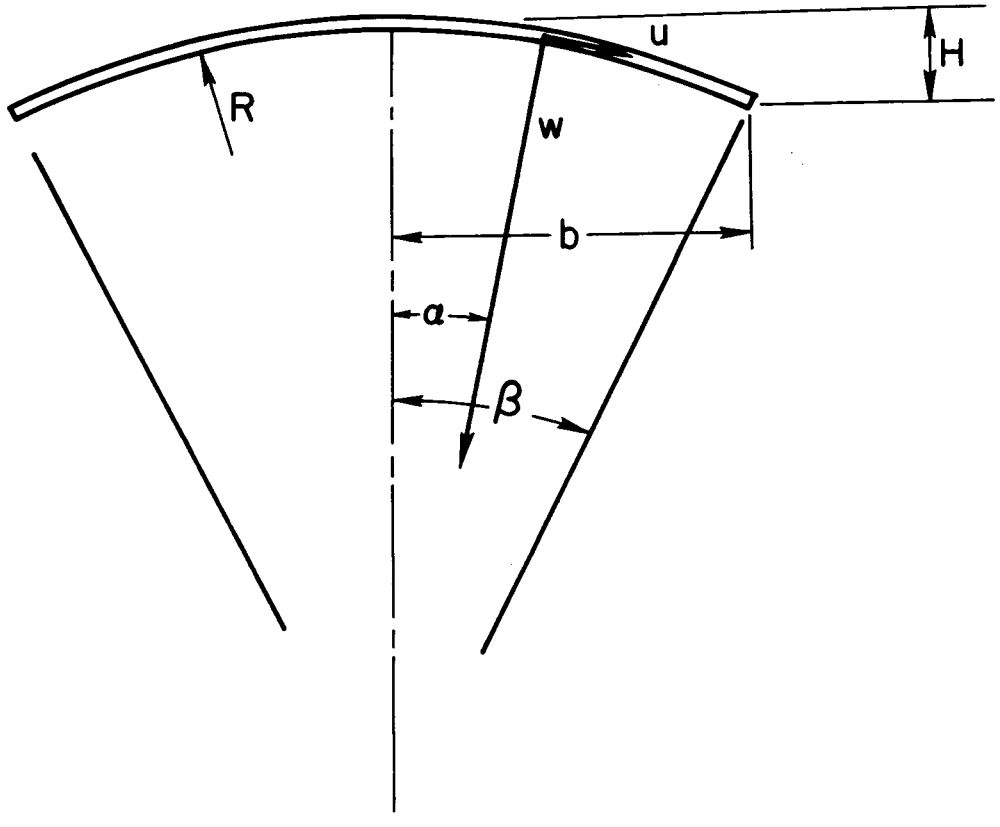

(b) Spherical cap.

Figure 7.- Concluded.

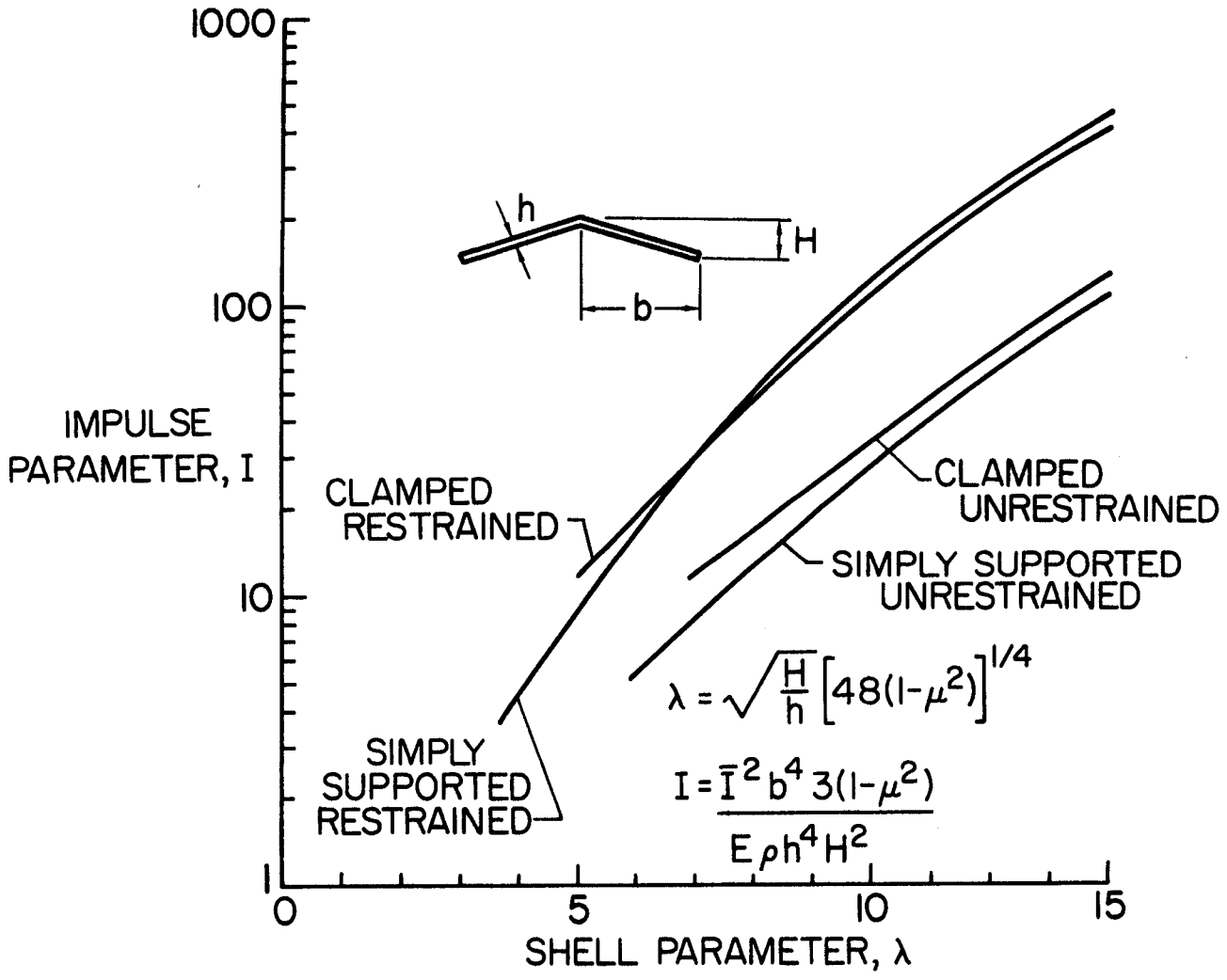

Figure 8.- Snap-through impulse versus shell parameter for axisymmetric shallow conical shells.

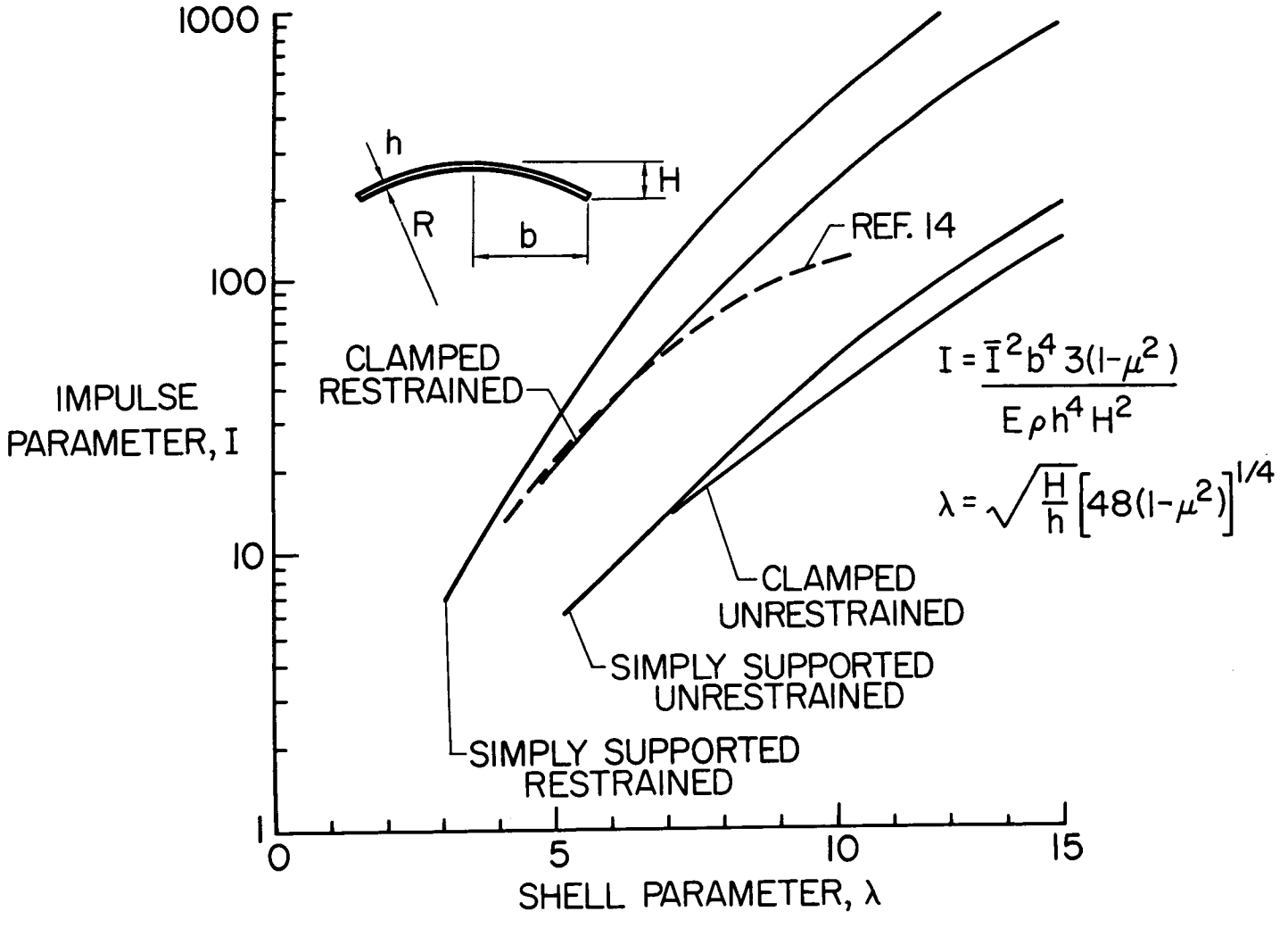

Figure 9.- Snap-through impulse versus shell parameter for axisymmetric shallow spherical shells.

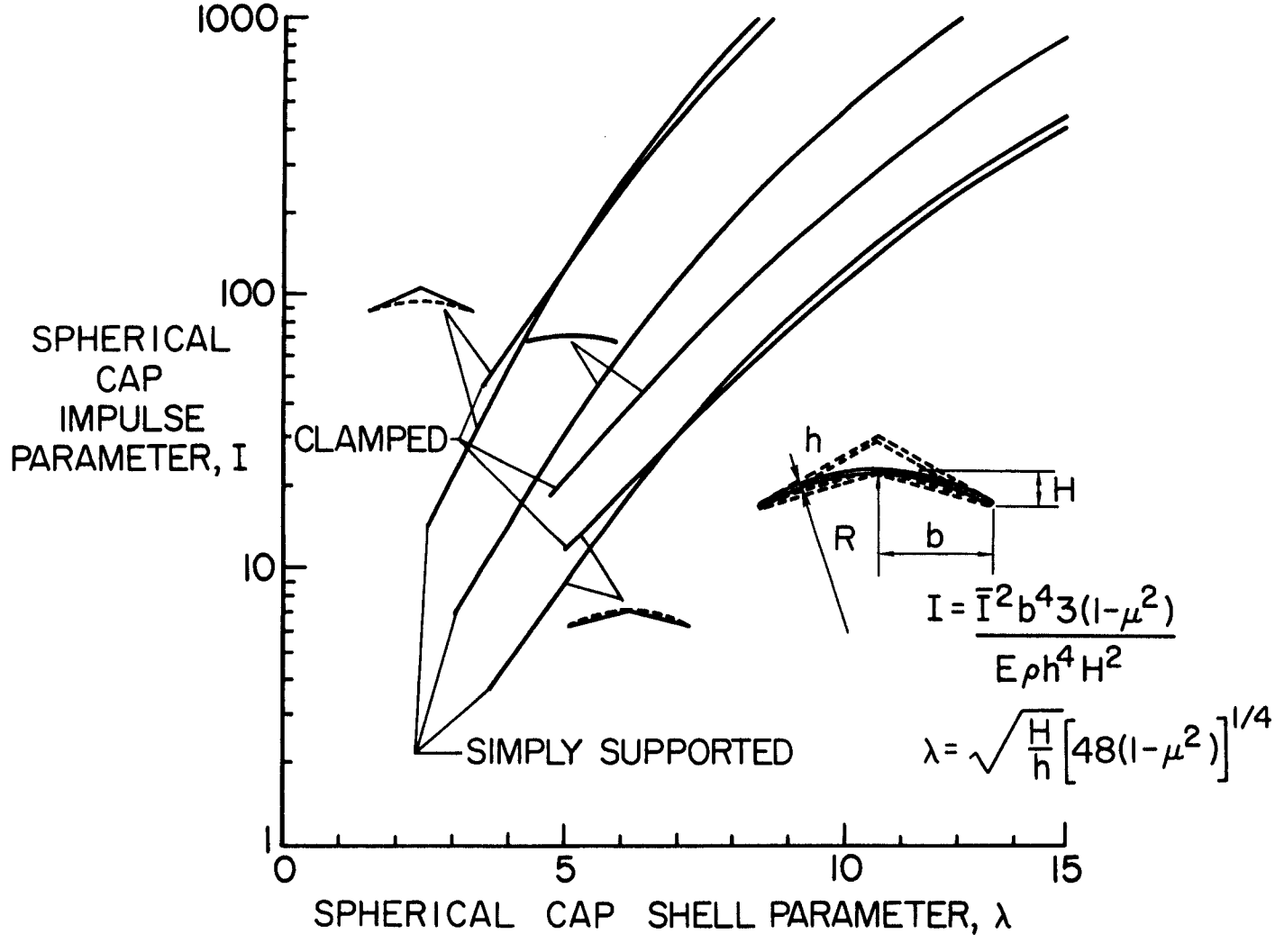

Figure 10.- Comparison of snap-through impulse for restrained spherical shell with conical shell.